THE JOURNAL OF BIOLOGICAL CHEMISTRY VOL. 280, NO. 52, pp. 43179–43187, December 30, 2005
Printed in the U.S.A.

Comparison of Structure and Dynamics of Micelle-bound Human α-Synuclein and Parkinson Disease Variants*[S]

Received for publication, July 13, 2005, and in revised form, September 8, 2005 Published, JBC Papers in Press, September 15, 2005, DOI 10.1074/jbc.M507624200

Tobias S. Ulmer[1] **and Ad Bax**[2]

From the Laboratory of Chemical Physics, NIDDK, National Institutes of Health, Bethesda, Maryland 20892

Three point mutations (A30P, E46K, and A53T) as well as gene triplication genetically link the 140-residue protein α-synuclein (aS) to the development of Parkinson disease. Here, the structure and dynamics of micelle-bound aS(A30P) and aS(A53T) are described and compared with wild-type aS, in addition to describing the aS-micelle interaction. A53T is sensed only by directly adjacent residues and leaves the backbone structure and dynamics indistinguishable from the wild type. A30P interrupts one helix turn (Val^{26}–Ala^{29}) and destabilizes the preceding one. A shift in helix register following A30P disturbs the canonical succession of polar and hydrophobic residues for at least two turns. The shortened helix-N adopts a slightly higher helical content and is less bent, indicating that strain was present in the micelle-bound helix. In the vicinity of the A30P-induced perturbations, the underlying micelle environment has rearranged, but nevertheless all aS variants maintain similar interrelationships with the micelle. Moreover, aS-micelle immersion correlates well with fast and slow aS backbone dynamics, allowing a rare insight into protein-micelle interplay.

Parkinson disease (PD)[3] is characterized by the selective demise of neurons of the substantia nigra pars compacta, leading to progressive motoric dysfunction (1–3). Cell death occurs as a result of the accumulation of intraneuronal inclusions known as Lewy bodies (ubiquinated protein deposits in the cytoplasm) and Lewy neurites (thread-like proteinaceous inclusions within neurites). Biochemical and histological analyses have identified the 140-residue protein α-synuclein (aS) to be a major component of Lewy bodies and Lewy neurites (4, 5). Furthermore, aS gene triplication as well as any of the mutations A30P, E46K, and A53T have been genetically linked to familial PD (6–9). At the molecular level, misfolding of aS into aggregates appears to be a common denominator in the pathogenesis of PD, which strongly correlates with age. Misfolding benefits from the impaired degradation of aS (10) and, in particular, oxidation of aS by reactive oxygen species (11, 12) created by impairments in mitochondrial complex I activity (11), caused, for example, by environmental toxins, and catalyzed by iron and copper. Moreover, the dopamine-containing neurons of the substantia nigra pars compacta exhibit a unique sensitivity to impairments in mitochondrial complex I activity (11).

In aqueous solution aS is predominantly unfolded but readily associates with small unilamellar vesicles (SUV) and micelles containing negatively charged lipids and detergents, respectively (13–16), supporting its association with presynaptic vesicles *in vivo* and rationalizing its localization primarily at axon termini (17, 18). In complex with SUV of 300–400 Å diameter, the repeat region of aS (Fig. 1) is likely to form a single, uninterrupted α-helix (19), whereas in complex with smaller diameter micelles the repeat region is partitioned into two anti-parallel α-helices, helix-N (Val^3–Val^{37}) and helix-C (Lys^{45}–Thr^{92}), with no detectable tertiary contacts, connected by a well ordered linker (20). The C-terminal tail of aS remains at all times free in solution, preceded, at least in the micelle-bound state, by a short extended region (Gly^{93}–Lys^{97}) (15, 16, 20). The one or more exact physiological functions of aS are still under investigation, but aS may be relevant for synaptic plasticity and neurotransmitter release (13, 21–24) in good agreement with the impact of aS binding on SUV or micelles (14, 20, 25, 26).

In aqueous solution aS can be induced to aggregate (27, 28), and Val^{71}–Val^{82} appear important in this respect (29). In the presence of certain lipid environments, which also induce α-helical structure, aggregation kinetics is accelerated even further (30–32). Moreover, in aqueous solution all three aS PD variants (A30P, E46K, and A53T) aggregate faster than wild-type aS (27, 30, 33–35). For the aS(A53T) variant a consensus exists that this mutation does not affect vesicle binding or aS helical content (36–38). The just recently identified aS(E46K) variant enhances liposome binding (34). In contrast, for the aS(A30P) variant lipid binding is decreased, although reports vary from only relatively small decreases (36, 37) to pronounced effects (18, 38).

For the pathogenesis of PD and related synucleopathies, a number of factors may synergistically contribute, based also on the overall genetic make-up and environmental factors of individuals. Of course, it is exceedingly difficult to comprehensively address PD pathogenesis and the current study merely characterizes the effects of the A30P and A53T substitutions on the structure and dynamics of wild-type aS when bound to micelles. As the here-employed solution NMR spectroscopy is limited by particle size, only micelle- rather than vesicle-bound aS can be studied. However, both A30P and A53T mutations lie within the two helices of micelle-bound aS that bear close structural resemblance to the vesicle-bound state (20), and the reported results are therefore expected to be relevant for the vesicle-bound state, too. Indeed, the vesicle-binding properties of the PD variants are readily rationalized by our findings. Examination of altered protein-micelle interactions between the different aS variants as well as delineation of their immersion into the micelle provides additional information on the effect of these mutations at the molecular level.

* This work was supported in part by the Intramural Research Program of the NIDDK, National Institutes of Health (NIH) and by the Antiviral Target Program of the Office of the Director, NIH. The costs of publication of this article were defrayed in part by the payment of page charges. This article must therefore be hereby marked "*advertisement*" in accordance with 18 U.S.C. Section 1734 solely to indicate this fact.

[S] The on-line version of this article (available at http://www.jbc.org) contains supplemental Figs. S1–S5.

[1] Supported by a Long-Term Fellowship from the Human Frontier Science Program Organization. To whom correspondence may be addressed. Present address: Zilkha Neurogenetic Institute and Dept. of Biochemistry and Molecular Biology, Keck School of Medicine, University of Southern California, 1501 San Pablo St. , Los Angeles, CA 90089-2821. Tel.: 323-442-4326; Fax: 323-442-2145; E-mail: tulmer@usc.edu.

[2] To whom correspondence may be addressed: Laboratory of Chemical Physics, NIDDK, National Institutes of Health, Building 5, Room B1-31, 5 Memorial Dr., Bethesda, MD 20892. Tel.: 301-496-2848; Fax: 301-402-0907; E-mail: bax@nih.gov.

[3] The abbreviations used are: PD, Parkinson disease; aS, human α-synuclein; MFR, molecular fragment replacement; HSQC, heteronuclear single quantum coherence; NMR, nuclear magnetic resonance; NOE, nuclear Overhauser effect; NOESY, NOE spectroscopy; RDC, residual dipolar coupling; SUV, small unilamellar vesicles; TROSY, transverse relaxation optimized spectroscopy; AMPS, 2-acrylamido-2-methyl-1-propanesulfonate.

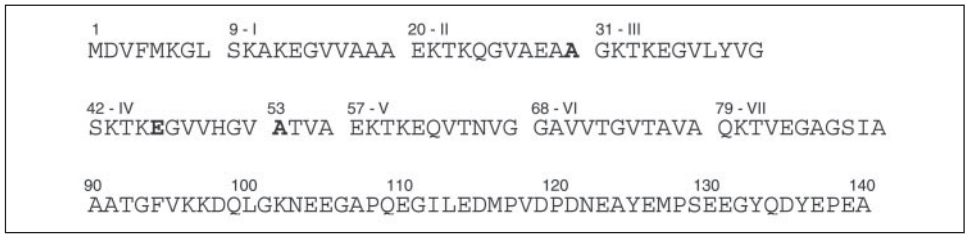

FIGURE 1. **Amino acid sequence of human α-synuclein (aS).** The seven imperfect 11-residue repeats of aS are labeled in *Roman numerals*. Residues Ala[30], Glu[46], and Ala[53], whose A30P, E46K, and A53T mutations are linked to familial Parkinson disease, are shown in *boldface*. Ser[9]–Ala[89] are referred to as the 'repeat region' and Asp[98]–Ala[140] as the 'tail region' of aS.

EXPERIMENTAL PROCEDURES

Protein Production—The human α-synuclein variants A30P and A53T were expressed from the kanamycin-restricted, T7*lac*-promoter-controlled pET-41 vector (Novagen) in *Escherichia coli* BL21(DE3) cells. M9 minimal medium (39) cultures, containing ^{2}H, ^{13}C, and ^{15}N enriched precursors, were grown, and the aS variants were purified to >98% purity as described for wild-type aS (20).

NMR Sample Preparation—Unless stated otherwise, all samples were prepared in H_2O to contain aS at a concentration of 0.5 mM ($\epsilon_{280} = 5120$ M^{-1} cm^{-1}), 75 mM SDS, 6% D_2O, 0.02% (w/v) NaN_3, and 20 mM NaH_2PO_4/Na_2HPO_4, pH 7.4, in a total volume of 270 μl. Besides isotropic samples, alignment of the protein-micelle complex relative to the magnetic field was achieved in the presence of stretched, negatively charged polyacrylamide gels (40, 41). Gels were polymerized from a 4.6% w/v solution of acrylamide, 2-acrylamido-2-methyl-1-propanesulfonate (AMPS), and bisacrylamide with a monomer to cross-linker ratio of 39:1 (w/w) and a molar ratio of 96:4 of acrylamide to AMPS, employing the previously described conventions and conditions (20).

NMR Spectroscopy—All experiments were carried out at 25 °C on Bruker spectrometers operating at ^{1}H frequencies of 600 and 800 MHz, equipped with cryogenic probes. Data were processed and analyzed with the NMRPipe package (42) and the program Xeasy (43). Throughout most experiments, the TROSY N–H component was selected (44, 45), and the solvent signal was returned to $+I_z$ before acquisition (46, 47). H^N, N, C^α, and C′ assignments were made from HNCA, HN(CO)CA, HNCO, HN(CA)CO, and HSQC-NOESY-TROSY experiments.

H^N–H^N NOEs were measured from HSQC-NOESY-TROSY experiments (τ_{mix} = 170 ms). $^{1}J_{NH}$, $^{1}J_{C\alpha C'}$, $^{1}J_{C'N}$, and $^{1}J_{NH}+^{1}D_{NH}$, $^{1}J_{C\alpha C'}+^{1}D_{C\alpha C'}$, $^{1}J_{C'N}+^{1}D_{C'N}$ couplings were determined from mixed-constant time, H^N-coupled HNCO (48), quantitative *J*-correlation HN(CA)CO (49), and quantitative *J*-correlation HNCO experiments (50) of isotropic and aligned samples, respectively. The ^{15}N relaxation parameters R_1, R_2, and $\{^{1}H\}$–^{15}N NOE were determined at 60.8 MHz (51, 52). For the $\{^{1}H\}$–^{15}N NOE measurement, 5 s of presaturation preceded by a recycling delay of 4 s were used for the NOE experiment and a 9-s recycle delay for the reference experiment.

Structure Calculation—In complete analogy to the aS wild-type structure calculation (20), backbone dihedral angle restraints were derived by molecular fragment replacement (MFR) (53, 54). Considering that large amplitude internal dynamics complicates such an analysis, MFR results are restricted to residues exhibiting generalized order parameters, S^2, above 0.6. The remaining residues are represented by random-coil conformations. A fragment length of seven residues was used during MFR (20). For the aS(A30P) variant, 278 N, C^α, and C′ chemical shifts and 261 $^{1}D_{NH}$, $^{1}D_{C\alpha C'}$, and $^{1}D_{C'N}$ RDCs were used; for the aS(A53T) variant these numbers were also 278 and 261, respectively. H^N–H^N internuclear distances were quantified from H^N–H^N NOE values using an empirical $1/r^{-4}$ dependence (55) for the ratio of diagonal- to cross-peak intensities, calibrated to a H^N_{i-1}–H^N_i distance of 2.8 Å within α-helical conformation. Although MFR yields well defined local geometry for structured regions that are mobile with respect to the main part of the protein, such mobility typically results in a reduction in magnitude of the local alignment tensor, D_a. Backbone torsion angles can therefore be obtained for the ordered part of the protein ($S^2 > 0.6$), but the relative orientation of structural elements with much reduced D_a values cannot be defined accurately by RDCs. Consequently, during structure calculations a global alignment tensor and RDCs were only used for residues within fragments exhibiting $D_a > 6$ Hz and $S^2 > 0.8$ (residues 9–21, 57–63, and 70–80 for A30P; residues 11–22, 50–62, and 71–79 for A53T). Based on essentially indistinguishable relative orientations of the N- and C-terminal helices from those previously observed in wild-type aS, the same interhelix distance restraints previously measured for wild-type aS on the basis of paramagnetic relaxation enhancements (20) were used in the structure calculations of A30P and A53T. Simulated annealing calculations were carried out using the program Xplor-NIH 2.9.5 (56), using a temperature gradient from 500 to 0 K, in the presence of empirical potentials of mean force for backbone-backbone hydrogen-bonding (57) and torsion angles (58). The energy-minimized average structures of aS(A30P) and aS(A53T), respectively, were calculated from the ensemble of twenty lowest energy structures.

SDS-protein Cross-relaxation Effects—The availability of deuterated wild-type aS and PD variants was used as an opportunity to detect cross-relaxation between protein backbone $^{1}H^N$ nuclei and the SDS protons in a straightforward manner. The ratio of H–N cross-peak intensities from TROSY spectra recorded with and without selective presaturation of a particular SDS resonance, I/I_0, was quantified. Experiments were recorded in an interleaved manner, and ^{15}N Boltzmann magnetization was eliminated by phase cycling. SDS exhibits four well resolved ^{1}H signals, corresponding to $(CH_2)_1$, $(CH_2)_2$, $(CH_2)_{3-11}$, and $(CH_2)_{12}$ (*cf.* the Spectral Data base for Organic Compounds, SDBS 2985HSP-46-269), which can be selectively irradiated. The employed presaturation (500 ms, $\gamma_H B_1 = 22$ Hz) of, for example, $(CH_2)_{3-11}$ attenuated the signal intensities of neighboring resonances $(CH_2)_1$, $(CH_2)_2$, and $(CH_2)_{12}$ by 25%, 15, and 40%, respectively. To assess any contribution from residual carbon-bonded protein protons, I/I_0 was also measured using deuterated SDS with presaturation of $(CH_2)_{3-11}$. An essentially random fluctuation with $I/I_0 = 0.995 \pm 0.009$ was obtained (supplemental Fig. S1), confirming the validity of the current approach.

SDS Titration—Titrations as a function of SDS concentration were performed in 20 mM NaH_2PO_4/Na_2HPO_4, pH 7.4/6% D_2O at 25 °C and 800 MHz. At each titration point a TROSY-HSQC spectrum was recorded with $t_{1,max}(^{15}N) = 145$ ms, $t_{2,max}(^{1}H^N) = 114$ ms, using final digital resolutions of 1.7 and 2.2 Hz/point, respectively. For both aS(A30P) and aS(A53T), starting protein concentrations were 0.2 mM. A total of 11 titration steps were performed for each sample, from molar aS:SDS ratios of 1:0 to 1:422. The first titration step was chosen at 2.8 mM SDS (aS:SDS = 1:14), just above its estimated critical micelle concentration of 2.6 mM (59). Between the titration steps corresponding to aS:SDS ratios of 1:14 and 1:43, complex spectral properties are obtained for resonances of the repeat region (20). Between aS:SDS ratios of 1:58

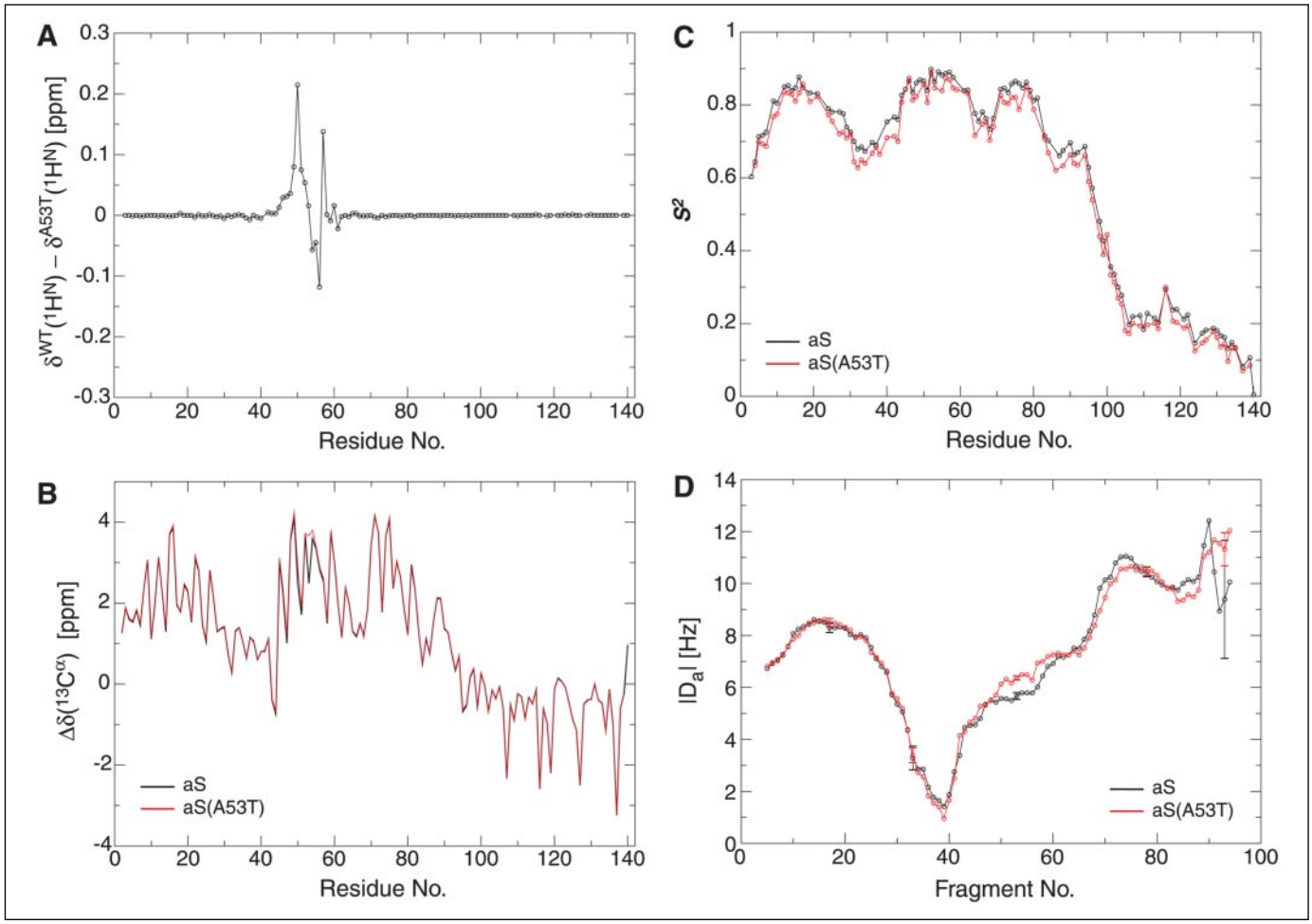

FIGURE 2. **Comparison of structural and dynamic parameters between the aS(A53T) variant and wild-type aS.** *A*, differences in amide proton ($^1H^N$) chemical shift between aS(A53T) and wild-type aS. *B*, difference in observed $^{13}C^\alpha$ chemical shift and tabulated random-coil values as a function of residue number, for both aS(A53T) (*red*) and wild-type aS (*black*). These so-called $^{13}C^\alpha$ secondary shifts are reported relative to the random coil values of Ref. 63 but have not been corrected for the ~+0.5 ppm isotope shift resulting from perdeuteration of the carbon-attached hydrogens. *C*, generalized order parameters, S^2, derived from backbone ^{15}N relaxation analysis using an isotropic model (79). In the presence of the unfolded tail of aS, an isotropic model was found to reproduce the relaxation data well (data not shown). If only residues in the structured region are considered for which relaxation parameters could be extracted for all three examined aS forms (54 residues), rotational correlation times, τ_c, of 15.8 ± 0.1 ns and 16.0 ± 0.1 ns are obtained for aS(A53T) and wild-type aS, respectively. Statistical errors in S^2 are smaller than the data symbols. *D*, variation of the absolute alignment tensor magnitude, D_a, obtained during molecular fragment replacement (MFR) using a fragment length of seven residues, along the sequence. The *fragment number* corresponds to the center residue of each 7-residue fragment. No unique local structure could be found for fragments involving the highly mobile tail residues, and therefore no D_a values are available for this region. To compensate for a slight variation in the alignment strength of the employed aligning media, the D_a values of aS(A53T) have been uniformly scaled to obtain a match with wild-type aS for the average D_a value of *fragments 10–20*. The root-mean-square deviation of D_a values for the ten best MFR fragments is shown as an *error bar* for selected, representative fragments.

and 1:422, peak positions change relatively little and assignments follow directly from those made at aS:SDS = 1:150.

RESULTS

Structure and Dynamics of aS(A53T) Are Essentially Indistinguishable from Wild-type aS—Chemical shifts of nuclei are sensitive probes of local structure and, in particular, differences in chemical shifts are highly sensitive indicators for differences in structure. Because each nucleus provides a unique reporter site, differences in structure between two proteins can be compared at numerous sites. Here, the chemical shift, δ, of the backbone amide proton ($^1H^N$) and the secondary shift of the $^{13}C^\alpha$ nucleus for each amino acid residue are compared between the aS(A53T) variant and wild-type aS. The $^1H^N$ chemical shift depends on the immediate chemical environment, including both local geometry and hydrogen bonding (60–62). $^{13}C^\alpha$ shifts depend most strongly on the backbone torsion angles ϕ and ψ (63), and the difference between the experimental $^{13}C^\alpha$ shift and tabulated random-coil values yields readily interpretable structural information.

Detectable $^1H^N$ shift differences between aS(A53T) and aS extend over approximately ±8 amino acid residues from the site of mutation (Fig. 2*A*). In agreement with the local α-helical secondary structure, the most pronounced $^1H^N$ shift changes are observed for the $^1H^N$ nuclei closest to the new side chain of residue 53, in particular those in positions −3, +3, and +4 from the site of mutation (Fig. 2*A*). Except for residues 53 and 54, $^{13}C^\alpha$ secondary shifts in aS(A53T) and aS are essentially the same (Fig. 2*B*). Small increases in $^{13}C^\alpha$ secondary shift for Thr^{53} and Thr^{54} in the mutant suggest the adoption of slightly higher local helical character compared with wild-type aS. However, when calculating the structure of the aS(A53T) variant, it was found to be indistinguishable from wild-type aS, as expected on the basis of the very similar chemical shifts for the remaining residues, and therefore warrants no further discussion.

The backbone dynamics of the aS(A53T) variant and wild-type aS are compared on two timescales. On a fast timescale (picosecond-nanosecond), the amplitude of the fluctuations of H–N bond vector orientations are reported by the generalized order parameter, S^2, which ranges from

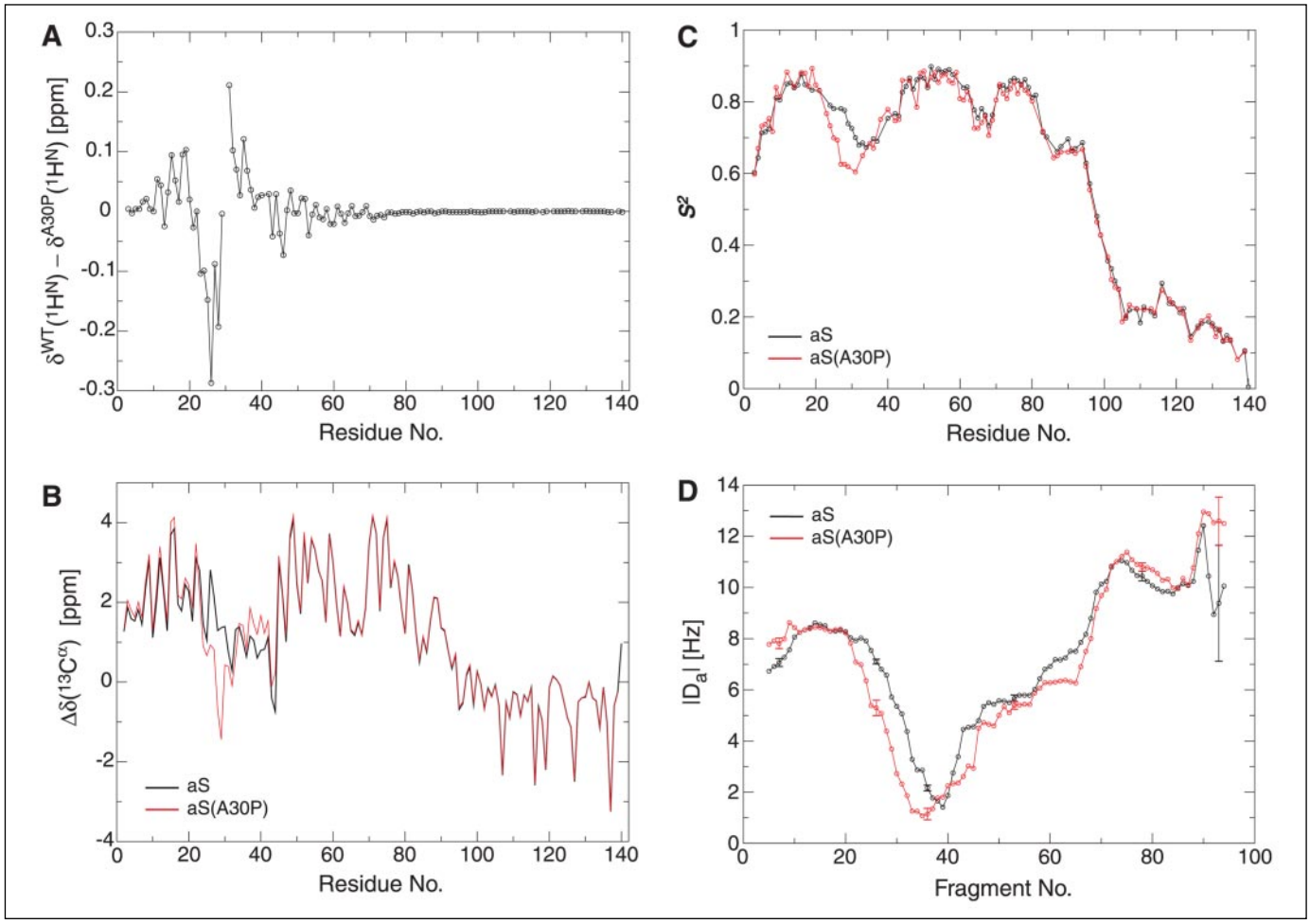

FIGURE 3. **Comparison of structural and dynamic parameters between the aS(A30P) variant and wild-type aS.** *A*, differences in amide proton ($^1H^N$) chemical shift between aS(A30P) and wild-type aS. *B*, differences in observed $^{13}C^\alpha$ chemical shift and tabulated random-coil values as a function of residue number for both aS(A30P) (*red*) and wild-type aS (*black*). These so-called $^{13}C^\alpha$ secondary shifts are reported relative to the random coil values of Ref. 63, but have not been corrected for the ~+0.5 ppm isotope shift resulting from perdeuteration of the carbon-attached hydrogens. *C*, generalized order parameters, S^2, derived from backbone ^{15}N relaxation analysis using an isotropic model (79). In the presence of the unfolded tail of aS, an isotropic model was found to reproduce the relaxation data well (data not shown). If only residues in the structured region are considered, for which relaxation parameters could be extracted for all three examined aS forms (54 residues), rotational correlation times, τ_c, of 15.1 ± 0.1 ns and 16.0 ± 0.1 ns are obtained for aS(A30P) and wild-type aS, respectively. Statistical errors in S^2 are *smaller* than the *data symbols*. *D*, variation of the absolute alignment tensor magnitude, D_a, obtained during molecular fragment replacement (MFR) using a fragment length of seven residues, along the sequence. The *fragment number* denotes the center residue of each fragment. No unique local structure could be found for fragments involving the highly mobile tail residues, and therefore no D_a values are available for this region. To compensate for a slight variation in the alignment strength of the employed aligning media, the D_a values of aS(A30P) have been uniformly scaled to obtain a match with wild-type aS for the average D_a value of *fragments 10–20*. The root-mean-square deviation of D_a values for the ten best MFR fragments is shown as an *error bar* for selected, representative fragments.

0 to 1 (64). Low values, such as those observed for the C-terminal tail of aS (Fig. 2*C*), report unstructured regions and *vice versa*. On an intermediate timescale (nanosecond-millisecond) the fluctuations of entire segments of backbone structure are reflected in the observed local alignment in an anisotropic medium (65–68), quantified here by the alignment tensor magnitude, D_a. When comparing two regions, a lower D_a value indicates the presence of larger amplitude dynamics relative the one with larger D_a. The backbone order, as represented by S^2, is found to be very similar for aS(A53T) and wild-type aS (Fig. 2*C*). The weak trend toward slightly lower S^2 values for aS(A53T) results in all likelihood from minor differences in sample conditions. The nanosecond-millisecond timescale dynamics of helix-N and the helix-helix connector, as expressed by D_a, are superimposable between aS(A53T) and aS (Fig. 2*D*). The slightly higher D_a values around the site of mutation suggest the possibility of a small rigidification of the helix and efficient micelle immersion of Thr^{53}, respectively, in agreement with the increased $^{13}C^\alpha$ secondary shift of Thr^{53} over Ala^{53}. The differences in D_a seen immediately following helix-C (Fig. 2*D*) reflect the high spread in the best-scoring MFR fragments, resulting in a high degree of uncertainty in D_a, as a consequence of the transition to less ordered backbone structure upon termination of the aS repeat region (Fig. 1). In conclusion, the structure and dynamics of aS(A53T) and wild-type aS are virtually indistinguishable.

The A30P Substitution Significantly Perturbs Wild-type aS Structure and Dynamics—The A30P substitution causes backbone $^1H^N$ chemical shift changes that extend well over ±30 residues from the site of mutation, into the helix-helix connector and helix-C (Fig. 3*A*). The largest $^1H^N$ shift changes are detected for Lys^{23}–Glu^{28} and Gly^{31}–Glu^{35}. The conformational space of a proline-preceding residue is restricted to extended conformations (69, 70) and, as anticipated, the largest difference in $^{13}C^\alpha$ secondary shifts is seen for the residue immediately preceding Pro^{30}, namely Ala^{29} (Fig. 3*B*). Even larger, negative $^{13}C^\alpha$ secondary shifts are also seen for the residues preceding the five prolines in the C-terminal tail of aS. The region of Val^{37}–Thr^{44}, *i.e.* up to the beginning of helix-C, shows the largest increases in $^{13}C^\alpha$ secondary shift, by ~0.5 ppm, whereas the $^1H^N$ shift changes in this region are moderate. Interestingly, for Glu^2–Thr^{22} the $^{13}C^\alpha$ secondary chemical shifts are slightly, but systematically elevated (Fig. 3*B*), indicating a very small increase in

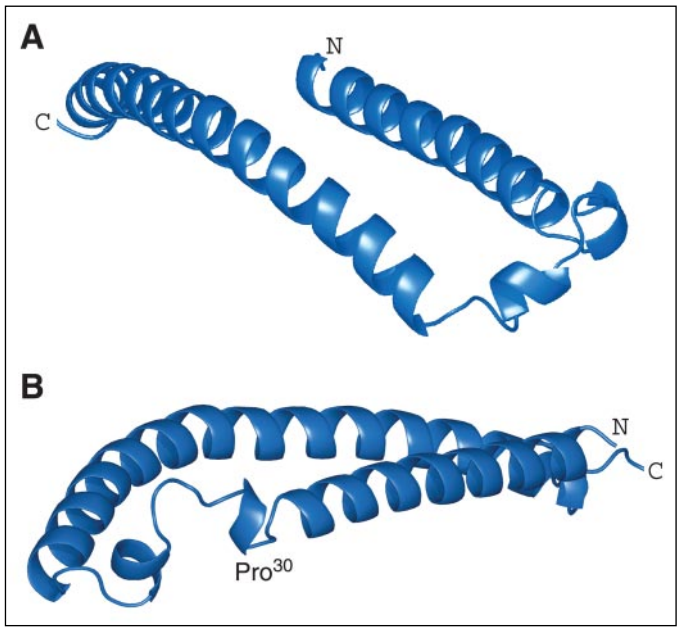

FIGURE 4. **Structure of micelle-bound aS(A30P).** *A* and *B*, *ribbon diagrams* illustrating the effective average secondary structures of aS(A30P). The complex tertiary structure between the two helices (Glu^{28}–Thr^{44}) could not be defined accurately (see main text). The dynamically disordered C-terminal tail has been omitted. The graphics were generated using PyMOL (W. L. DeLano (2002), www.pymol.org, DeLano Scientific, San Carlos, CA).

helical character. Nevertheless, the backbone order of aS(A30P) only differs from the wild-type outside experimental uncertainties for Gln^{24}–Lys^{32} (Fig. 3*C*). A clear decrease in S^2 is obtained for this region, indicating a destabilization of local secondary structure compared with wild-type aS.

Inspection of the wild-type structure (20) shows that Thr^{22}, Val^{26}, Ala^{29}, and Thr^{33} are in positions that contact the micelle surface. As a consequence of the forced transition of Ala^{29} in aS(A30P) from helical to extended conformation, Ala^{27}–Glu^{28} incur the largest decrease in S^2, by ~0.2, whereas Ala^{29} and Val^{26} exhibit somewhat smaller drops (Fig. 3*C*). Although the preceding helix turn (Thr^{22}–Gly^{25}) also shows signs of destabilization (Fig. 3*C*), Thr^{22}, flanked by Lys^{21} and Lys^{23}, is again indistinguishable from the wild type. The intermediate timescale dynamics, which is also sensitive to movements of entire stretches of secondary structure, shows an overall similar trend, with pronounced decreases in D_a for Thr^{22}–Gly^{36}, but a noteworthy difference is the slight increase in D_a at the beginning of helix-N′, possibly related to its reduced strain (Fig. 3*D*). Moreover, on the intermediate timescale, enhanced dynamics compared with the wild type are observed for more residues after Pro^{30} than on the fast timescale (Fig. 3, *C* and *D*). The effect of the A30P mutation extends in the C-terminal direction over a substantial distance, as discussed in more detail in the next section.

Another important consequence of the Pro-induced, extended conformation of Ala^{29} is an ensuing shift in register of the amphiphilic helix by (at least) one (Fig. 4). This brings the canonical succession of residues to contact the micelle surface out of order, *i.e.* the succession of hydrophobic and polar residues is disturbed (Fig. 1) and seems responsible for not seeing higher $^{13}C^{\alpha}$ secondary chemical shifts compared with wild-type aS before Val^{37} (Fig. 3*B*). The residues in Val^{37}-Leu-Phe-Val-Gly^{41} are all hydrophobic and as such not overly sensitive to a shift in helix register, again permitting better defined helical conformation. However, interestingly, the boundary of helix-C does not change to incorporate one or two more turns of helix. Rather, as was also seen in wild-type aS, the more hydrophilic residues Lys^{43}-Thr^{44} clearly interrupt helical propensity before helix-C commences (Fig. 3*B*), whose $^{13}C^{\alpha}$ secondary shifts are indistinguishable from the wild type, as also applies for the mostly unstructured C-terminal tail.

The unusually strong intermediate timescale dynamics of the aS-micelle system make the structure calculation of the aS(A30P) variant particularly difficult. Although information on the secondary structure elements present was obtained by MFR (53, 54), it did not prove accurate for defining the complex tertiary structure of residues Glu^{28}–Thr^{44}. Thus, only an illustrative picture of the effective, average secondary structure of aS(A30P) can be given (Fig. 4), which fails to accurately define the tertiary structure of Glu^{28}–Thr^{44}. The two helices of micelle-bound aS(A30P) are again found in an anti-parallel orientation. As a consequence of the A30P substitution, helix-N (Val^3–Val^{37}) terminates at Ala^{27} instead of Val^{37}, but Asp^2 is now also classified as α-helical (71) and Asp^2–Ala^{27} are referred to as helix-N′. The isomerization state of Pro^{30} is *trans* and is well defined, with no minor resonances visible for residues in the vicinity of Pro^{30}. This contrasts to some of the prolines in the C-terminal tail of aS, where minor conformers indicative of *cis* peptide bonds are clearly present (data not shown). The radius-of-curvature (R_C) of helix-N′ is 133 Å, and this helix is considerably less curved than Val^3–Ala^{27} of helix-N of the wild-type, which exhibits an R_C of 89 Å. The number of residues per turn, which is rather insensitive to helix curvature (72), is found to be 3.60 ± 0.06 for helix-N′ *versus* 3.63 ± 0.10 for Val^3–Ala^{27} of helix-N in wild-type aS. Helix-C (Lys^{45}–Thr^{92}) exhibits very similar, strong curvature in aS(A30P) and wild-type aS, with radii of curvature of 45 Å and 41 Å, respectively. For reasons already discussed for the aS(A53T) variant, MFR results are not unique for the transition from helix-C into the following extended tail region of aS (Fig. 3*D*). However, as there are no chemical shift changes in this region between aS(A30P) and the wild-type protein (Fig. 3, *A* and *B*), any structural changes can be safely excluded and the MFR fragments of the wild type, which have been selected using a larger number of restraints (20), are used for this region.

The Micelle Rearranges Slightly in Response to the A30P Mutation—The structure of wild-type aS in complex with a SDS micelle as well as the amino acid sequence of aS itself suggest that protein-micelle complex formation, and concomitant aS structuring from random-coil conformations seen in water, is driven by both hydrophobic and electrostatic interactions (13, 20). In particular, burial of the mostly hydrophobic face of helix-N and -C into the hydrophobic tail region of the micelle (73, 74) in combination with electrostatic interactions between the numerous Lys side chains, lining the sides of these helices, and the negatively charged detergent headgroups (75) stabilize the interaction. The electrostatic repulsion between detergent sulfate headgroups will be partially neutralized by the amino groups of these Lys residues and thus impact the shape of the micelle (20, 76). Indeed, a change in micelle shape upon aS binding may contribute to the relatively close, anti-parallel arrangement of the two aS helices (20). To have the deformation-inducing helices close to each other on one side of the micelle, in an arrangement where they exert similar directional forces on the micelle surface, is expected to be energetically least costly. Based on these arguments, a small change in micelle shape can be expected for aS(A30P) compared with wild-type aS, whereas for aS(A53T) no such change is expected.

First, it is noted that aS-micelle complex formation for aS(A53T) and aS(A30P) is indistinguishable from wild-type aS, as shown by a titration as a function of SDS concentration (supplemental Fig. S3). For the wild-type complex formation is essentially complete at a molar aS:SDS ratio of 1:70 (15, 20). Secondly, the isotropic correlation times, τ_c, obtained from ^{15}N relaxation analysis for the (same) subset of structured residues

of aS at aS:SDS = 1:150, for the different aS-micelle complexes are with 16.0 ± 0.1, 15.8 ± 0.1, and 15.1 ± 0.1 ns for wild-type aS, aS(A53T), and aS(A30P), respectively, rather similar. The τ_c reports on the (effective) overall particle size and, thus, the τ_c values show that the effects of the A30P and A53T substitutions on the micelle size are small. The small difference in τ_c of aS(A30P) compared with wild-type aS and aS(A53T) is noteworthy, but because the hydrodynamic properties and shape of the aS-micelle particle are strongly influenced by the highly acidic, dynamically unstructured tail of aS, no quantitative interpretation of the small differences in τ_c values can be provided.

To now detect subtle changes in micelle shape from the viewpoint of aS, the different sensitivities of $^1H^N$ chemical shifts and $^{13}C^\alpha$ secondary shifts to structural changes are exploited. The absence of a change in $^{13}C^\alpha$ secondary shift in the presence of a change in $^1H^N$ chemical shift at a given residue indicates alterations in the "outside" structural environment, including side-chain conformation, rather than the backbone. As discussed above, for the aS(A53T) variant the $^1H^N$ chemical shift differences to wild-type aS (Fig. 2*A*) can be attributed to the presence of the new Thr side chain. For the aS(A30P) variant, helix-C exhibits readily detectable $^1H^N$ shift changes without concomitant $^{13}C^\alpha$ secondary shift changes (Fig. 3, *A* and *B*). The long-range nature of the $^1H^N$ shift changes, up to residue 70, cannot be explained by a propagation of A30P-induced structural changes along the protein backbone, but rather must arise through a subtle change in the interaction with the underlying micelle environment, *i.e.* a slight rearrangement of detergent molecules, resulting from the structural and dynamic perturbations created by A30P (Figs. 3 and 4). As a consequence of the anti-parallel arrangement of helix-N and -C, only the beginning of helix-C shows $^1H^N$ shift changes, whereas after residue 70 no shift changes are observed (Fig. 3*A*).

The chemical shift changes shown in Figs. 2 and 3 are obtained at a molar aS:SDS ratio of 1:150. It is of some interest to confirm the long-range $^1H^N$ chemical shift changes also at other protein:SDS ratios. For example, at an aS:SDS ratio of 1:58 a single resonance is observed for each backbone N–H group of aS, and the obtained spectrum already closely resembles the micelle-saturated state (20), indicating that the aS helices are well developed at this stage. However, at this substoichiometric aS:micelle ratio, two aS molecules will be bound to some of the micelles, and the observed small differences in chemical shift relative to the micelle-saturated state are expected to arise largely from shifting all aS molecules to become single micelle tenants. Although it is difficult to relate these shift changes to particular structural events, a comparison between wild-type aS and the PD variants nevertheless identifies differences arising from alterations in protein-micelle interactions. For the aS(A53T) variant no significant changes compared with the wild-type were observable (Fig. 5*A*). In contrast, for aS(A30P) clear differences were obtained in helix-N and at the beginning of helix-C (Fig. 5*B*), supporting a subtle change in micelle interaction for these regions relative to the wild type.

The aS Micelle Immersion Varies and Correlates with Structural and Dynamic aS Parameters—The structural and dynamic parameters of micelle-bound aS vary significantly along the sequence (Figs. 2, 3, and 5). To what extent can this be rationalized by local differences in micelle immersion? Within the deuterated protein environment of aS, its micelle immersion is most readily studied by examining cross-relaxation effects between the aS backbone $^1H^N$ nuclei and the different SDS ^1H nuclei. Out of the twelve hydrocarbons of SDS three give well resolved ^1H signals, $(CH_2)_1$, $(CH_2)_2$, and $(CH_3)_{12}$, whereas the remaining nine, $(CH_2)_{3-11}$, coincide (data not shown), thus providing the opportunity to study aS-micelle immersion at four different positions/regions

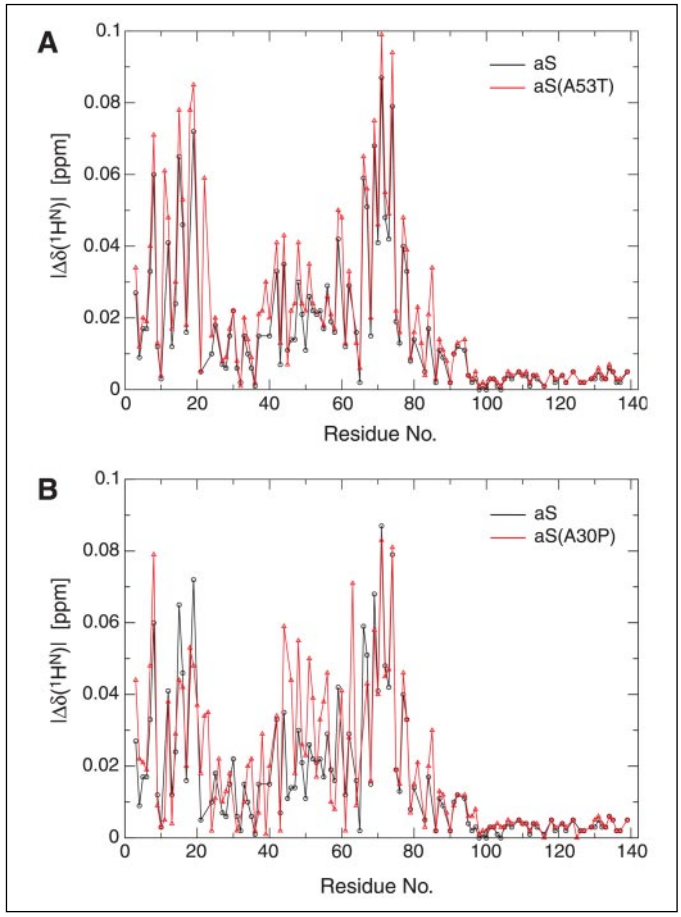

FIGURE 5. **aS chemical shift changes upon populating a single micelle from higher order complexes.** Comparison of aS absolute $^1H^N$ chemical shift changes between molar aS:SDS ratios of 1:58 and 1:422 for: *A*, wild-type aS (*black*) and aS(A53T) (*red*); *B*, wild-type aS (*black*) and aS(A30P) (*red*). A 1:1 complex between aS and a micelle is formed from an aS to SDS ratio of ~1:70 onward (15, 20) (supplemental Fig. S3).

along the SDS tail. As a measure of cross-relaxation effects, the ratio of the N–H signal intensity, of each aS residue in the presence and absence of selective presaturation of a particular SDS signal, I/I_0, is evaluated.

Effects following presaturation of $(CH_2)_{3-11}$ are most pronounced, whereas for $(CH_3)_{12}$ irradiation the smallest variation in I/I_0 ratios is observed (Fig. 6 and supplemental Fig. S4). Substantial effects from $(CH_2)_1$ or $(CH_2)_2$ irradiation are rare, but distinct (Fig. 6). To illustrate the immersion pattern, the I/I_0 ratios for cross-relaxation originating on $(CH_2)_{3-11}$ are shown *color-coded* on the average structure of wild-type aS embedded in a putative ellipsoid micelle (Fig. 7). With the exception of the second half of helix-N, the structure can be placed within an ideal prolate ellipsoid micelle to satisfactorily explain the I/I_0 ratios. The apparent absence of significant micelle immersion for the second half of helix-N is in agreement with the absence of significant chemical shift changes of this region upon populating a single micelle from higher order complexes (Fig. 5). Moreover, Ala^{30}–Val^{37} of helix-N exhibit reduced helical character, relatively low order parameters (Fig. 3*C*), and fast exchange of their $^1H^N$ nuclei with the solvent (20), indicating their proximity to the solvent layer of the micelle. A small deformation of an ideal ellipsoid micelle near the second half of helix-N can account for these structural and dynamic properties. In addition, this region, together with the helix-helix connector, is highly dynamic on the intermediate timescale, demonstrating a highly dynamic environment for entire secondary structure elements and suggesting that any deformation of the micelle would be highly dynamic, too. Gln^{65}–Ala^{69} and

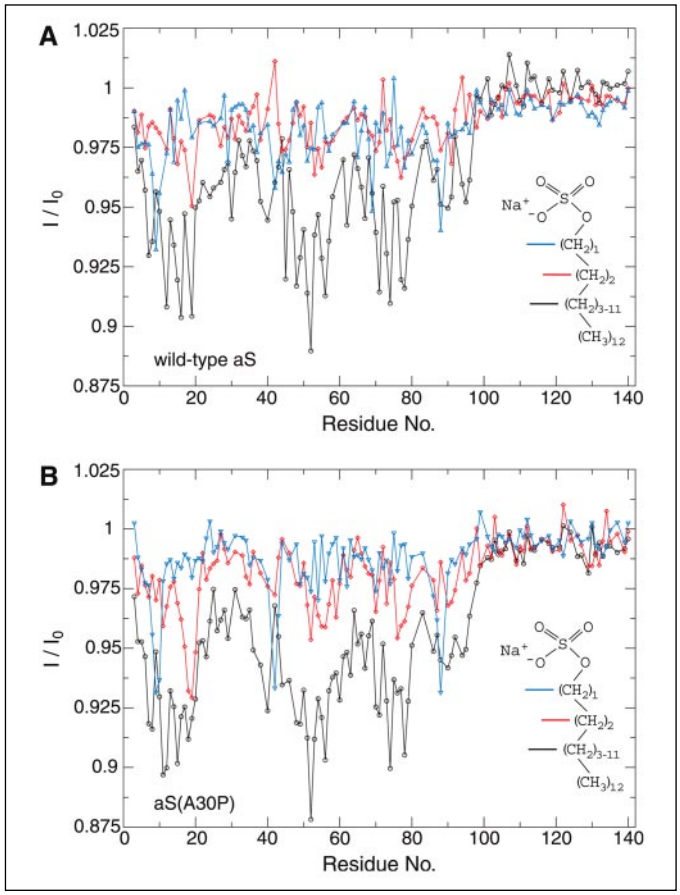

FIGURE 6. **aS-micelle cross-relaxation effects.** Signal intensity ratios of H–N resonances of: *A*, wild-type aS; *B*, the aS(A30P) variant recorded with and without presaturation, I/I_0, of selected SDS resonances, as indicated in the figure.

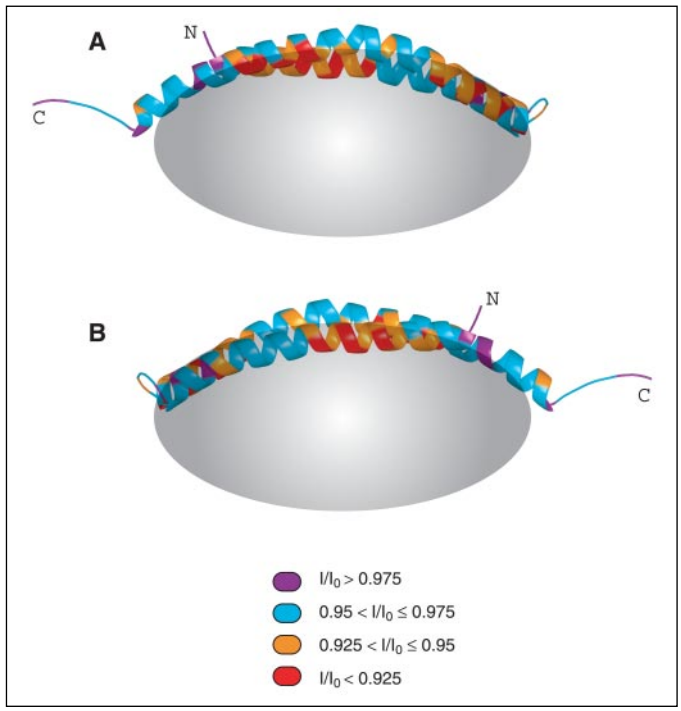

FIGURE 7. **Illustration of aS micelle immersion.** Signal intensity ratios, I/I_0, obtained upon presaturation of $(CH_2)_{3-11}$ of SDS (Fig. 6*A*) shown *color-coded* on the average structure of wild-type aS (PDB ID 1XQ8). Gaps in I/I_0 ratios of Fig. 6*A*, arising from resonance overlap, have been interpolated. The structure is shown embedded in an ellipsoid micelle (axes ratio 2:1). Views *A* and *B* are related by a 180° rotation around the vertical axis. The graphics were generated using PyMOL.

Gly^{84}–Ser^{87} also readily exchange with the solvent (20) and exhibit pronounced fast timescale dynamics (Fig. 3*C*) in excellent agreement with their relatively high I/I_0 ratios (Fig. 6*A*) and placement relative to the micelle (Fig. 7). In conclusion, the micelle immersion of aS correlates particularly well with fast and slow aS backbone dynamics as well as SDS titration data, demonstrating their intimate interrelatedness and a high degree of self-consistency of our data. In passing, it is noted that the residues of helix-C that are close to the micelle surface (Fig. 7) are particularly well suited for the attachment of paramagnetic tags.

The rare effects from $(CH_2)_1$ or $(CH_2)_2$ irradiation are interesting in their own right. They mostly occur when the protein backbone tends to surface from within deeper regions represented by $(CH_2)_{3-11}$ (Fig. 6). Within a putative ellipsoid micelle (Fig. 7), the orientation of the hydrocarbon tails of SDS relative to each other will vary widely, which may contribute to some of the smaller variations in I/I_0 ratios and differences between $(CH_2)_1$, $(CH_2)_2$, and $(CH_2)_{3-11}$ (Fig. 6). The I/I_0 pattern following $(CH_2)_{3-11}$ irradiation is overall complementary to effects obtained when adding paramagnetic ions directly to a solution of micelle-bound aS (74). Slightly larger variations to the current data are apparent when adding spin-labeled stereates to the micelle itself (73).

Between wild-type aS and the PD variants the obtained I/I_0 ratios are, within experimental errors, quite similar (Fig. 6 and supplemental Fig. S5). The aS(A30P) variant shows only slight differences to the other two forms in the vicinity of the site of mutation. The immersion pattern of Val^{37}–Thr^{44} is interesting in this context: the sequence Val^{37}-Leu-Phe-Val^{40} submerges before Ser^{42}-Lys-Thr^{44} resurfaces again, following their hydrophobic and hydrophilic natures, respectively. For aS(A30P) this pattern seems more pronounced than for the wild type, suggesting that the A30P-induced helix break allows slightly more favorable interactions with the detergent molecules in this region. But overall the A30P substitution takes place in a region that is not deeply immersed into the micelle in the first place (Fig. 6), and the long range effects on the chemical shifts (Figs. 3*A* and 5) suggest that the micelle rearranges to optimize the immersion of aS(A30P).

DISCUSSION

For wild-type aS, we previously showed that the chemical shifts and thereby the structure of the protein are relatively insensitive to the type of detergent used (anionic SDS *versus* zwitterionic dodecyl phosphocholine) (20), and the favorable aS spectral characteristics observed in SDS are therefore used in the present comparison of aS with its PD mutants. In the micelle- or vesicle-bound states of wild-type aS, the side chain of Ala^{53} points "sideways" from the aS helix, *i.e.*, parallel to the micelle or vesicle surface (20). As expected for such an orientation, the backbone structure and dynamics of the aS Parkinson disease (PD) variant A53T are found to be virtually unchanged from the wild type. The presence of the new Thr side chain is reflected in backbone amide proton ($^1H^N$) chemical shift changes for residues in positions −3, +3, and +4 from the site of mutation, characteristic of α-helical conformation. The A53T substitution has no adverse effect on helix stability, neither on a sub-nanosecond nor on a nano- to microsecond timescale. In fact, increased $^{13}C^\alpha$ secondary shifts relative to wild type for Thr^{53}-Thr^{54} indicate a small increase in local helical character at the site of mutation. This observation is interesting in light of the fact that a substitution of Thr for Ala is often a destabilizing α-helical conformation (77). Within a helix, the β-branched side chain of Thr is restricted to *trans* conformations: an entropic cost that is not present for Ala. A favorable enthalpic interaction attained for the Thr side chain in the context of the

micelle environment must be compensating for the entropic cost of A53T.

The side chain of Ala^{30} in wild-type aS also points sideways, but in the aS(A30P) variant the substitution to Pro impacts the backbone. It restricts the conformational space available to the preceding residue, Ala^{29}, which directly faces the micelle surface in wild-type aS, to extended conformations (69–78), implying the loss of two intrahelical hydrogen bonds (78). Although certain combinations of *X*-Pro residues can form a favorable C-terminal helix cap, Ala-Pro is not one of them (70). Thus, based on arguments for helices of globular proteins, the A30P substitution will lead to an interruption and destabilization of helix-N (Val^3–Val^{37}). On the other hand, in micelle-bound wild-type aS, residues Ala^{30}–Val^{37} already exhibit a lower helical character than helix-C or the other residues of helix-N, and the helices are significantly bent (20). An A30P-induced helix break therefore provides an opportunity for helix-N to relieve curvature strain, and for the residues following Pro^{30} to repartition and even to shift the boundary to helix-C (Lys^{45}–Thr^{92}).

The C-terminal tail and helix-C of aS(A30P) present themselves essentially indistinguishable from the wild type. The impact of A30P reaches the boundary to helix-C, as judged by $^1H^N$ and $^{13}C^\alpha$ chemical shift changes relative to the wild type, but, interestingly, leaves it unchanged. An important factor for this behavior may be the hydropathicities of the residues preceding helix-C. The hydrophobic stretch Val^{37}–Val^{40} is found to immerse distinctly into the micelle, and its RDCs are compatible with helical conformation, whereas the hydrophilic stretch Ser^{42}–Thr^{44} surfaces again and its RDCs are indicative of extended conformation. The residues immediately following A30P up to Gly^{36} are highly dynamic but exhibit a tendency toward helix formation, which may enable the, on average, α-helical conformation of Val^{37}–Val^{40}, which contrasts with the wild-type structure (20). The shortened helix-N′ starts at Glu^2 and terminates at Ala^{27}; Glu^{28} and in particular Ala^{29} are "pushed" toward extended conformations by the ring of Pro^{30} (78), which faces the micelle. Residues Asp^2–Thr^{22} benefit from the A30P-induced helix break by adopting a slightly, but systematically, higher helical content, as shown by slightly higher $^{13}C^\alpha$ secondary shifts compared with wild type, whereas the remainder of helix-N′ (Lys^{23}–Ala^{27}) is destabilized as reflected by its dynamic parameters caused by the A30P substitution. Helix-N′ is only slightly bent (radius of curvature $R_C = 133$ Å), particularly compared with helix-N of the wild-type ($R_C = 76$ Å, or 89 Å when only considering Val^3–Ala^{27}), indicating that helix strain was present in helix-N. This finding agrees with the notion that aS prefers to bind to vesicles of certain diameters (14) and, thus, will preferentially stabilize these vesicles, which may relate to the possible physiological functions of aS (13, 21–24).

The here reported structure and dynamics of micelle-bound aS and the PD variants aS(A30P) and aS(A53T) provide a structural basis for their vesicle-binding properties. For aS(A53T) no significant structural and dynamic changes compared with the wild-type are detected, in agreement with the absence of changes in vesicle binding (36–38). The interruption of one helix turn, destabilization of another one, and the register shift following the A30P substitution create a larger perturbation. However, given the many hydrophobic contacts (1 every 3.6 residues) and at least 9 lysine-detergent headgroup contacts, these disturbances are still relatively small, supporting only small perturbations in vesicle binding (36, 37). The third PD mutation, E46K, increases the ability of aS to bind to negatively charged liposomes (34). This result is readily rationalized based on the micelle-bound aS structure (20): Glu^{46} points sideways from helix-C, and E46K positions another lysine residue to favorably interact with a negatively charged lipid headgroup.

As a corollary to the above notion that strain has been relieved from helix-N′ following A30P, it can be expected that the micelle shape has changed somewhat, too. Small, but readily detectable, long range $^1H^N$ shift changes in helix-C of aS(A30P) compared with wild-type aS at several aS:SDS ratios, in the absence of concomitant backbone structural changes ($^{13}C^\alpha$ shift changes), provide support for this conclusion. It should be noted, however, that a small change in micelle shape is inseparably intertwined with a small change in protein-micelle interaction. A titration of aS(A30P) with SDS shows no loss in micelle binding compared with the wild type, and the aS(A30P) micelle immersion pattern is overall quite similar to the wild type, suggesting that a small rearrangement of detergent molecules can well accommodate the altered structure and dynamics of aS(A30P), *i.e.* the aS(A30P)-micelle system arrives at a similar free energy as the wild-type one. In the presence of vesicles rather than micelles, it has been reported that the unbound form of aS increases from 14 ± 2% for wild-type aS to 36 ± 3% for the aS(A30P) variant (37), showing that a lipid bilayer accommodates defects in the helical pattern of aS less well than a micelle or, in other words, a lipid bilayer is less dynamic than a micelle. Of course, lipids within a bilayer possess a higher order than detergents within a micelle and, consequently, the ability to change shape is much more restricted for the bilayer. Thus, the micelle and aS clearly influence each other's geometry. In particular, the reduced curvature of helix-N′ over helix-N shows that the micelle prefers to be less flat than the aS helices would like it to be, and vice versa.

The micelle immersion pattern of aS is in excellent agreement with fast (picosecond to nanosecond) and slow (millisecond to second) timescale aS backbone dynamics as well as aS chemical shift changes upon populating a single micelle from higher order complexes. The variations in slow and fast timescale dynamics have been previously related to the distribution of Gly residues within the aS helices (20). The stretches of aS that immerse well into the micelle show little cross-relaxation of their backbone amide protons to the first two hydrocarbons of the SDS detergent tail. Rather, effects are strongest for cross-relaxation to the tail region comprising hydrocarbons 3–11, whose chemical shifts overlap and therefore do not allow a further differentiation. From data using micelles doped with spin-labeled stereates, it was suggested that aS immersion, which is ultimately limited by the negatively charged functional groups on the "upper" side of the aS helices, is no deeper than hydrocarbon 4 (74). Taken together, this places the aS immersion depth near hydrocarbons 3 and 4, and brings some of the negatively charged side chains lining the upper side of the aS helices close to the sulfate headgroups of the detergent. Moreover, this shows that, within the helical segment, residues at all positions of the aS repeat region bear relevance for its interaction with vesicle membranes or micelles, although residues lining the "lower" side of the aS helices are most critical. The highly conserved nature of synuclein proteins is noted in this context. In summary, the immersion of aS into synaptic membranes will not only impact their fluidity, but also influence their surface charge distribution, creating a distinct "signature" at the membrane-water interface.

Acknowledgments—The aS(A30P) and aS(A53T) expression vectors were kindly provided by Nelson Cole and Robert Nussbaum. We thank Alexander Grishaev, Frank Delaglio, Nelson Cole, and Robert Nussbaum for helpful discussions.

REFERENCES

1. Vekrellis, K., Rideout, H. J., and Stefanis, L. (2004) *Mol. Neurobiol.* **30,** 1–21
2. Norris, E. H., Giasson, B. I., and Lee, V. M. Y. (2004) *Stem Cells Dev. Dis.* **60,** 17–54
3. Nussbaum, R. L., and Ellis, C. E. (2003) *N. Engl. J. Med.* **348,** 1356–1364
4. Spillantini, M. G., Schmidt, M. L., Lee, V. M. Y., Trojanowski, J. Q., Jakes, R., and

Goedert, M. (1997) *Nature* **388,** 839–840
5. Mezey, E., Dehejia, A. M., Harta, G., Suchy, S. F., Nussbaum, R. L., Brownstein, M. J., and Polymeropoulos, M. H. (1998) *Mol. Psychiatry* **3,** 493–499
6. Kruger, R., Kuhn, W., Muller, T., Woitalla, D., Graeber, M., Kosel, S., Przuntek, H., Epplen, J. T., Schols, L., and Riess, O. (1998) *Nat. Genet.* **18,** 106–108
7. Singleton, A. B., Farrer, M., Johnson, J., Singleton, A., Hague, S., Kachergus, J., Hulihan, M., Peuralinna, T., Dutra, A., Nussbaum, R., Lincoln, S., Crawley, A., Hanson, M., Maraganore, D., Adler, C., Cookson, M. R., Muenter, M., Baptista, M., Miller, D., Blancato, J., Hardy, J., and Gwinn-Hardy, K. (2003) *Science* **302,** 841
8. Polymeropoulos, M. H., Lavedan, C., Leroy, E., Ide, S. E., Dehejia, A., Dutra, A., Pike, B., Root, H., Rubenstein, J., Boyer, R., Stenroos, E. S., Chandrasekharappa, S., Athanassiadou, A., Papapetropoulos, T., Johnson, W. G., Lazzarini, A. M., Duvoisin, R. C., DiIorio, G., Golbe, L. I., and Nussbaum, R. L. (1997) *Science* **276,** 2045–2047
9. Zarranz, J. J., Alegre, J., Gomez-Esteban, J. C., Lezcano, E., Ros, R., Ampuero, I., Vidal, L., Hoenicka, J., Rodriguez, O., Atares, B., Llorens, V., Tortosa, E. G., del Ser, T., Munoz, D. G., and de Yebenes, J. G. (2004) *Ann. Neurol.* **55,** 164–173
10. Cuervo, A. M., Stefanis, L., Fredenburg, R., Lansbury, P. T., and Sulzer, D. (2004) *Science* **305,** 1292–1295
11. Dawson, T. M., and Dawson, V. L. (2003) *Science* **302,** 819–822
12. Cole, N. B., Murphy, D. D., Lebowitz, J., Di Noto, L., Levine, R. L., and Nussbaum, R. L. (2005) *J. Biol. Chem.* **280,** 9678–9690
13. George, J. M., Jin, H., Woods, W. S., and Clayton, D. F. (1995) *Neuron* **15,** 361–372
14. Davidson, W. S., Jonas, A., Clayton, D. F., and George, J. M. (1998) *J. Biol. Chem.* **273,** 9443–9449
15. Chandra, S., Chen, X. C., Rizo, J., Jahn, R., and Sudhof, T. C. (2003) *J. Biol. Chem.* **278,** 15313–15318
16. Eliezer, D., Kutluay, E., Bussell, R., and Browne, G. (2001) *J. Mol. Biol.* **307,** 1061–1073
17. Iwai, A., Masliah, E., Yoshimoto, M., Ge, N. F., Flanagan, L., Desilva, H. A. R., Kittel, A., and Saitoh, T. (1995) *Neuron* **14,** 467–475
18. Jensen, P. H., Nielsen, M. S., Jakes, R., Dotti, G., and Goedert, M. (1998) *J. Biol. Chem.* **273,** 26292–26294
19. Jao, C. C., Der-Sarkissian, A., Chen, J., and Langen, R. (2004) *Proc. Natl. Acad. Sci. U. S. A.* **101,** 8331–8336
20. Ulmer, T. S., Bax, A., Cole, N. B., and Nussbaum, R. (2005) *J. Biol. Chem.* **280,** 9595–9603
21. Abeliovich, A., Schmitz, Y., Farinas, I., Choi-Lundberg, D., Ho, W. H., Castillo, P. E., Shinsky, N., Verdugo, J. M. G., Armanini, M., Ryan, A., Hynes, M., Phillips, H., Sulzer, D., and Rosenthal, A. (2000) *Neuron* **25,** 239–252
22. Ellis, C. E., Schwartzberg, P. L., Grider, T. L., Fink, D. W., and Nussbaum, R. L. (2001) *J. Biol. Chem.* **276,** 3879–3884
23. Cabin, D. E., Shimazu, K., Murphy, D., Cole, N. B., Gottschalk, W., McIlwain, K. L., Orrison, B., Chen, A., Ellis, C. E., Paylor, R., Lu, B., and Nussbaum, R. L. (2002) *J. Neurosci.* **22,** 8797–8807
24. Murphy, D. D., Rueter, S. M., Trojanowski, J. Q., and Lee, V. M. Y. (2000) *J. Neurosci.* **20,** 3214–3220
25. Nuscher, B., Kamp, F., Mehnert, T., Odoy, S., Haass, C., Kahle, P. J., and Beyer, K. (2004) *J. Biol. Chem.* **279,** 21966–21975
26. Ramakrishnan, M., Jensen, P. H., and Marsh, D. (2003) *Biochemistry* **42,** 12919–12926
27. Conway, K. A., Harper, J. D., and Lansbury, P. T. (1998) *Nat. Med.* **4,** 1318–1320
28. Hashimoto, M., Hsu, L. J., Sisk, A., Xia, Y., Takeda, A., Sundsmo, M., and Masliah, E. (1998) *Brain Res.* **799,** 301–306
29. Giasson, B. I., Murray, I. V. J., Trojanowski, J. Q., and Lee, V. M. Y. (2001) *J. Biol. Chem.* **276,** 2380–2386
30. Perrin, R. J., Woods, W. S., Clayton, D. F., and George, J. M. (2001) *J. Biol. Chem.* **276,** 41958–41962
31. Cole, N. B., Murphy, D. D., Grider, T., Rueter, S., Brasaemle, D., and Nussbaum, R. L. (2002) *J. Biol. Chem.* **277,** 6344–6352
32. Narayanan, V., and Scarlata, S. (2001) *Biochemistry* **40,** 9927–9934
33. Narhi, L., Wood, S. J., Steavenson, S., Jiang, Y. J., Wu, G. M., Anafi, D., Kaufman, S. A., Martin, F., Sitney, K., Denis, P., Louis, J. C., Wypych, J., Biere, A. L., and Citron, M. (1999) *J. Biol. Chem.* **274,** 9843–9846
34. Choi, W., Zibaee, S., Jakes, R., Serpell, L. C., Davletov, B., Crowther, R. A., and Goedert, M. (2004) *FEBS Lett.* **576,** 363–368
35. Greenbaum, E. A., Graves, C. L., Mishizen-Eberz, A. J., Lupoli, M. A., Lynch, D. R., Englander, S. W., Axelsen, P. H., and Giasson, B. I. (2005) *J. Biol. Chem.* **280,** 7800–7807
36. Perrin, R. J., Woods, W. S., Clayton, D. F., and George, J. M. (2000) *J. Biol. Chem.* **275,** 34393–34398
37. Bussell, R., and Eliezer, D. (2004) *Biochemistry* **43,** 4810–4818
38. Jo, E. J., Fuller, N., Rand, R. P., St George-Hyslop, P., and Fraser, P. E. (2002) *J. Mol. Biol.* **315,** 799–807
39. Sambrook, J., and Russell, D. W. (2001) *Molecular Cloning: A Laboratory Manual*, 3rd Ed., p. A2.1, Cold Spring Harbor Laboratory Press, Cold Spring Harbor, NY
40. Tycko, R., Blanco, F. J., and Ishii, Y. (2000) *J. Am. Chem. Soc.* **122,** 9340–9341
41. Ulmer, T. S., Ramirez, B. E., Delaglio, F., and Bax, A. (2003) *J. Am. Chem. Soc.* **125,** 9179–9191
42. Delaglio, F., Grzesiek, S., Vuister, G. W., Zhu, G., Pfeifer, J., and Bax, A. (1995) *J. Biomol. NMR* **6,** 277–293
43. Bartels, C., Xia, T. H., Billeter, M., Guntert, P., and Wuthrich, K. (1995) *J. Biomol. NMR* **6,** 1–10
44. Pervushin, K., Riek, R., Wider, G., and Wuthrich, K. (1997) *Proc. Natl. Acad. Sci. U. S. A.* **94,** 12366–12371
45. Weigelt, J. (1998) *J. Am. Chem. Soc.* **120,** 10778–10779
46. Grzesiek, S., and Bax, A. (1993) *J. Am. Chem. Soc.* **115,** 12593–12594
47. Ulmer, T. S., Campbell, I. D., and Boyd, J. (2004) *J. Magn. Reson.* **166,** 190–201
48. Cornilescu, G., and Bax, A. (2000) *J. Am. Chem. Soc.* **122,** 10143–10154
49. Jaroniec, C. P., Ulmer, T. S., and Bax, A. (2004) *J. Biomol. NMR* **30,** 181–194
50. Chou, J. J., Delaglio, F., and Bax, A. (2000) *J. Biomol. NMR* **18,** 101–105
51. Farrow, N. A., Muhandiram, R., Singer, A. U., Pascal, S. M., Kay, C. M., Gish, G., Shoelson, S. E., Pawson, T., Formankay, J. D., and Kay, L. E. (1994) *Biochemistry* **33,** 5984–6003
52. Zhu, G., Xia, Y. L., Nicholson, L. K., and Sze, K. H. (2000) *J. Magn. Reson.* **143,** 423–426
53. Delaglio, F., Kontaxis, G., and Bax, A. (2000) *J. Am. Chem. Soc.* **122,** 2142–2143
54. Kontaxis, G., Delaglio, F., and Bax, A. (2005) *Methods Enzymol.* **394,** 42–78
55. Guntert, P., Braun, W., and Wuthrich, K. (1991) *J. Mol. Biol.* **217,** 517–530
56. Schwieters, C. D., Kuszewski, J. J., Tjandra, N., and Clore, G. M. (2003) *J. Magn. Reson.* **160,** 65–73
57. Grishaev, A., and Bax, A. (2004) *J. Am. Chem. Soc.* **126,** 7281–7292
58. Kuszewski, J. J., and Clore, G. M. (2000) *J. Magn. Reson.* **146,** 249–254
59. Brito, R. M. M., and Vaz, W. L. C. (1986) *Anal. Biochem.* **152,** 250–255
60. Oldfield, E. (2002) *Annu. Rev. Phys. Chem.* **53,** 349–378
61. Wishart, D. S., and Case, D. A. (2001) *Methods Enzymol.* **338,** 3–34
62. Cordier, F., and Grzesiek, S. (1999) *J. Am. Chem. Soc.* **121,** 1601–1602
63. Spera, S., and Bax, A. (1991) *J. Am. Chem. Soc.* **113,** 5490–5492
64. Lipari, G., and Szabo, A. (1982) *J. Am. Chem. Soc.* **104,** 4546–4559
65. Meiler, J., Prompers, J. J., Peti, W., Griesinger, C., and Bruschweiler, R. (2001) *J. Am. Chem. Soc.* **123,** 6098–6107
66. Tolman, J. R., Al-Hashimi, H. M., Kay, L. E., and Prestegard, J. H. (2001) *J. Am. Chem. Soc.* **123,** 1416–1424
67. Deschamps, M., Campbell, I. D., and Boyd, J. (2005) *J. Magn. Reson.* **172,** 118–132
68. Bouvignies, G., Bernado, P., and Blackledge, M. (2005) *J. Magn. Reson.* **173,** 328–338
69. Karplus, P. A. (1996) *Protein Sci.* **5,** 1406–1420
70. Prieto, J., and Serrano, L. (1997) *J. Mol. Biol.* **274,** 276–288
71. Anderson, C. A. F., Palmer, A. G., Brunak, S., and Rost, B. (2002) *Structure* **10,** 175–184
72. Kumar, S., and Bansal, M. (1998) *Biophys. J.* **75,** 1935–1944
73. Bisaglia, M., Tessari, I., Pinato, L., Bellanda, M., Giraudo, S., Fasano, M., Bergantino, E., Bubacco, L., and Mammi, S. (2005) *Biochemistry* **44,** 329–339
74. Bussell, R., Ramlall, T. F., and Eliezer, D. (2005) *Protein Sci.* **14,** 862–872
75. Montserret, R., McLeish, M. J., Bockmann, A., Geourjon, C., and Penin, F. (2000) *Biochemistry* **39,** 8362–8373
76. Garg, G., Hassan, P. A., Aswal, V. K., and Kulshreshtha, S. K. (2005) *J. Phys. Chem. B* **109,** 1340–1346
77. Fersht, A. (1999) *Structure and Mechanism in Protein Science*, W. H. Freeman and Company, New York
78. Richardson, J. S., and Richardson, D. C. (1989) in *Prediction of Protein Structure and the Principles of Protein Conformation* (Fasman, G. D., ed) pp. 1–89, Plenum Press, New York
79. Dosset, P., Hus, J. C., Blackledge, M., and Marion, D. (2000) *J. Biomol. NMR* **16,** 23–28